JPE 18-4-26

https://doi.org/10.6113/JPE.2018.18.4.1245
ISSN(Print): 1598-2092 / ISSN(Online): 2093-4718

Droop Control Scheme of a Three-phase Inverter for Grid Voltage Unbalance Compensation

Hongpeng Liu†, Jiajie Zhou*, Wei Wang*, and Dianguo Xu*

†,*Department of Electrical Engineering, Harbin Institute of Technology, Harbin, China

Abstract

The stability of a grid-connected system (GCS) has become a critical issue with the increasing utilization of renewable energy sources. Under grid faults, however, a grid-connected inverter cannot work efficiently by using only the traditional droop control. In addition, the unbalance factor of voltage/current at the common coupling point (PCC) may increase significantly. To ensure the stable operation of a GCS under grid faults, the capability to compensate for grid imbalance should be integrated. To solve the aforementioned problem, an improved voltage-type grid-connected control strategy is proposed in this study. A negative sequence conductance compensation loop based on a positive sequence power droop control is added to maintain PCC voltage balance and reduce grid current imbalance, thereby meeting PCC power quality requirements. Moreover, a stable analysis is presented based on the small signal model. Simulation and experimental results verify the aforementioned expectations, and consequently, the effectiveness of the proposed control scheme.

Key words: Active power, Droop control, Grid-connected inverter, Negative sequence, Positive sequence, Reactive power, Unbalance compensation

I. INTRODUCTION

A serious unbalanced grid voltage condition results when a high-capacity single-phase or unbalanced three-phase load connects to a grid. Nevertheless, the common controller of a three-phase grid-connected inverter is mostly designed for the condition of a three-phase balanced grid. Therefore, grid imbalance generates many issues, such as inverter output current distortion, negative sequence component increase of inverter output voltage, and low-frequency fluctuation of injection power. In addition, grid imbalance may affect the safe and stable operation of local loads connected to the common coupling point (PCC). Standards have been developed to limit the range of grid imbalance. The International Electrical Commission (IEC) recommends that voltage unbalance in three-phase systems should be limited to 2%. In GB/T 15543-2008, the negative voltage unbalance factor (VUF) of a grid should be less than 2% under the normal operation of a grid and should not exceed 4% in a short period [1]. VUF is defined as the ratio of the negative sequence voltage component to the positive sequence voltage component, i.e.,

$$VUF = \frac{V_{PCC}^{-}}{V_{PCC}^{+}} \times 100\% \,. \tag{1}$$

Recently, approaches have been proposed to achieve unbalance voltage compensation at PCC. Among these approaches, the current control scheme is widely adopted. Reference [2] proposed a double current loop control scheme in which the positive and negative sequence components of grid current are controlled under the positive and negative synchronization reference frames, respectively. However, a low-pass filter is required to extract the DC component of the d–q axis current [3]. The delay induced by the filter affects the control accuracy and stability of a system. A full-feedforward scheme was proposed to reduce the injected grid-current harmonics and unbalance caused by grid voltage [4]. However, the control scheme was implemented in the synchronous d–q frame, which requires power decoupling control in the d- and q-axes. In [5], five different strategies were presented to generate inverter reference currents according to the corresponding unbalance control requirements. In the case of balanced positive-sequence control, currents are sinusoidal and

Manuscript received Oct. 27, 2017; accepted Mar. 3, 2018
Recommended for publication by Associate Editor Jongbok Baek.
†Corresponding Author: lhp602@hit.edu.cn
Tel: +86-451-86403230, Fax: +86-451-86413420, Harbin Inst. of Tech.
*Dept. of Electrical Eng., Harbin Institute of Technology, China

balanced although the positive-sequence component of grid voltage is used only to calculate grid current references. However, each control strategy achieves only one control objective (i.e., cancelling oscillations in power or obtaining sinusoidal current). A flexible grid voltage support strategy was proposed in [6]. The output positive-sequence voltage increases, whereas the output negative-sequence voltage decreases by adjusting the current reference. However, the voltage at PCC is indirectly compensated for by adjusting the line current, such that the compensation voltage highly depends on the line impedance of a microgrid. Thus, a small or unknown line impedance cannot achieve the expected grid voltage compensation effect. An enhanced instantaneous power theory for unbalanced three-phase four-wire or grounded systems was proposed in [7]. Active and reactive power can be kept constant by generating the instantaneous current reference.

Droop control is widely used in microgrids to achieve seamless transfer between islanded and grid-connected modes. The droop method is a voltage-controlled technique that maps the terminal parameters of a generator onto its active and reactive power generations [8]-[11]. However, grid voltage imbalance compensation is barely considered in droop-controlled inverters. *G*–*H* and Q^{-}–*G* droop controls have been introduced to share harmonics and unbalanced currents among distributed generation (DG) units. Reference [12] proposed a control strategy that comprised a voltage control loop, a droop controller, and a negative-sequence output impedance controller (NSIC). The voltage control loop and droop controller are respectively used to regulate load voltage and to share average power among DG units. The NSIC is used to adjust the negative-sequence output impedance of DG units, such that the negative-sequence currents of power lines are minimized. The aforementioned methods achieve good performance and improve the overall power quality of a system. However, these methods do not apply to operation in grid-connected mode. A microgrid hierarchical control strategy that considers complex line impedance was proposed in [13]. Microgrids can provide positive- and negative- sequence powers, support grid voltage, and ride through the voltage dip during the entire fault period by using a two-layer control structure. However, the control method requires a high-speed communication line in the micro-network to exchange voltage imbalance information at PCC, which increases system cost and control complexity. In [14], an improved scheme that dynamically varies the positive- and negative-sequence current reference limits, which can significantly reduce fault current to less than 1.5 p.u, was proposed. However, the control structure, including the zero-sequence loop, is too complicated for application to a digital control system.

In the current study, the vector relationship between the positive- and negative-sequence voltage and current is presented, and the compensation principle of PCC voltage is analyzed.

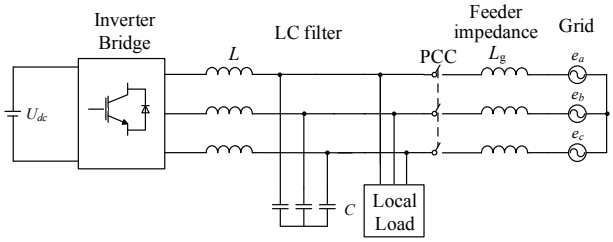

Fig. 1. Three-phase grid-connected inverter.

A negative-sequence reactive power conductance (Q^{-}–*G*) loop, which improves unbalanced voltage compensation at PCC, is introduced to the control system. In addition, the small-signal model is developed to evaluate the stability of the inverter.

The rest of the paper is organized as follows. Section II provides a brief analysis of the voltage and current vectors under an imbalanced grid condition. Section III describes droop control in grid-connected mode. Section IV analyzes the improved imbalance voltage compensation scheme. Section V presents the simulation and experimental results. Section VI draws the conclusions of the study.

II. Vector Analysis of Voltage and Current Under an Unbalanced Grid Condition

When three-phase voltage suffers from an asymmetrical fault, the voltage vector can be decomposed into positive-, negative-, and zero-sequence components based on the symmetrical component method [15]. The relevant expressions can be written as

$$\begin{cases} U_a = U_{a+} + U_{a-} + U_{a0} \\ U_b = U_{b+} + U_{b-} + U_{b0} \\ U_c = U_{c+} + U_{c-} + U_{c0} \end{cases}, \tag{2}$$

where U_{a+}, U_{b+}, and U_{c+} are positive-sequence components, U_{a-}, U_{b-}, and U_{c-} are negative-sequence components, and U_{a0}, U_{b0}, U_{c0} are zero-sequence components. As shown in Fig. 1, only the positive- and negative-sequence components are analyzed in this study because no zero-sequence current path exists in the three-phase three-wire system [16].

The results of the output voltage expressions of the inverter can be obtained by applying Kirchhoff's voltage law to the stationary reference frame in (3).

$$\begin{cases} v_\alpha = v_{g\alpha} + L_g \dfrac{di_\alpha}{dt} \\ v_\beta = v_{g\beta} + L_g \dfrac{di_\beta}{dt} \end{cases}, \tag{3}$$

where $v_{g\alpha}$ and $v_{g\beta}$ are grid voltages, v_α and v_β are inverter output voltages (voltages at PCC), i_α and i_β are injected grid current, and L_g is the line impedance between the grid and the inverter. In this study, only the inductive impedance is considered. The positive- and negative-sequence components

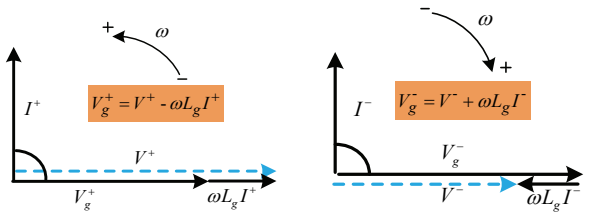

(a) (b)

Fig. 2. Vector representation of reactive power compensation: (a) Positive sequence, (b) Negative sequence.

of the grid voltage can be obtained as

$$\begin{cases} V_g^+ = V^+ - \omega L_g I^+ \\ V_g^- = V^- + \omega L_g I^- \end{cases}, \tag{4}$$

where V^+ and V^- are the positive- and negative-sequence components of the inverter output voltage, respectively; and ω is the angular frequency. The positive- and negative-sequence components of the inverter output current are

$$\begin{cases} I^+ = \dfrac{2}{3}\dfrac{Q^+}{V^+} \\ I^- = \dfrac{2}{3}\dfrac{Q^-}{V^-} \end{cases}. \tag{5}$$

From (4) and (5), the injected positive- and negative-sequence reactive powers can adjust the positive and negative components of the inverter output voltage, respectively. A high output positive reactive power indicates a high positive output voltage. A high output negative reactive power indicates a low negative output voltage. That is, the unbalance factor of PCC voltage is reduced.

The positive-sequence voltage V_g^+ decreases, and the negative-sequence voltage V_g^- increases due to the existence of unbalanced voltage. Therefore, the purpose of reactive power compensation is to increase the positive-sequence PCC voltage amplitude and decrease the magnitude of the negative-sequence PCC voltage by injecting reactive power Q [17].

Fig. 2 presents the phasor diagram to illustrates the reactive power compensation principle. V_g^+ rotates counterclockwise at 100π rad/s, whereas V_g^- turns clockwise. The initial phases of V_g^+ and V_g^- are assumed to be φ^+ and φ^-, respectively. Positive-sequence reactive power is analyzed first. As shown in Fig. 2(a), the positive-sequence reactive current I^+ is 90° ahead of V_g^+. The generating voltage drop across the line impedance is $\omega L_g I^+$, which lags behind I^+ by 90°. The positive-sequence PCC voltage V^+ is the sum of V_g^+ and $\omega L_g I^+$. Thus, the injection of the positive-sequence reactive power leads to an increase in PCC positive-sequence voltage component. Similarly, the PCC negative voltage V^- is the difference between V_g^- and $\omega L_g I^-$. The injection of the negative-sequence reactive power decreases the PCC negative-sequence voltage component.

If only a positive-sequence reactive power is injected into the grid, then the voltage unbalance factor can be reduced to a certain extent. However, the introduction of the positive-sequence reactive power may lead to overvoltage in one phase, as shown in Fig. 2(a). By contrast, if only a negative-sequence reactive power is injected into the grid, then undervoltage may occur in one phase. Therefore, by simultaneously injecting positive- and negative-sequence reactive powers, PCC voltage unbalance can be compensated and PCC voltage can be increased within the safe operation range (0.85 p.u to 1.10 p.u. in this study).

III. Analysis Droop Control in Grid-connected Mode

In accordance with instantaneous power theory [18], three-phase instantaneous active power p and reactive power q can be expressed as

$$\begin{cases} p = u_\alpha i_\alpha + u_\beta i_\beta \\ q = u_\beta i_\alpha - u_\alpha i_\beta \end{cases}, \tag{6}$$

where u_α and u_β and i_α and i_β are two-phase fundamental voltages and currents under a two-phase stationary coordinate system, respectively. The calculated p and q contain DC and AC components, respectively. The fundamental positive-sequence active power P^+ and reactive power Q^+ are DC components and can be obtained using a low-pass filter.

The fundamental positive-sequence components of voltage and current can be obtained based on the second-order generalized integrator [19]. The positive-sequence components of P^+ and Q^+ can be expressed as

$$P^+ = u_\alpha^+ i_\alpha^+ + u_\beta^+ i_\beta^+, \tag{7}$$

$$Q^+ = u_\beta^+ i_\alpha^+ - u_\alpha^+ i_\beta^+, \tag{8}$$

where u_α^+ and u_β^+ and i_α^+ and i_β^+ are positive-sequence voltages and currents in a two-phase stationary coordinate system, respectively.

When line impedance is inductive, the traditional P–f and Q–U droop expressions are

$$f = f_0 - k_p(P - P_0), \tag{9}$$

$$U = U_0 - k_q(Q - Q_0), \tag{10}$$

where f and U are the frequency and output voltage amplitude references, respectively; f_0 and U_0 are the rated frequency and output voltage amplitude of the inverter, respectively; P_0 and Q_0 are its rated active and reactive powers, respectively; P and Q are the calculated active and reactive powers, respectively; and k_p and k_q are the active and reactive droop coefficients, respectively.

Droop control requires the system to dynamically adjust the active and reactive power outputs to control the amplitude and phase of the output voltage. In an actual grid-connected system, small fluctuations are frequently observed in voltage

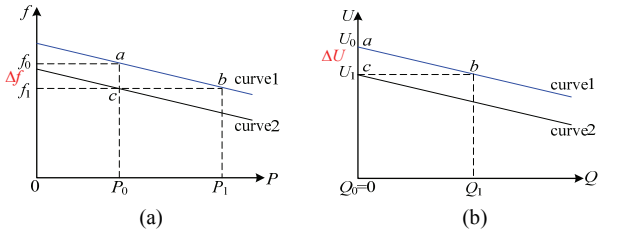

Fig. 3. Droop lines that illustrate: (a) Active power, (b) Reactive power fluctuations.

amplitude and frequency. Therefore, the traditional droop expression in (9) and (10) is not directly applicable and must be changed accordingly. One direct approach is to shift the droop curves, and the shift value is given in (11) and (12).

$$\Delta f_0 = (k_{pp} + \frac{k_{ip}}{s})(P_0 - P), \tag{11}$$

$$\Delta U_0 = (k_{pq} + \frac{k_{iq}}{s})(Q_0 - Q), \tag{12}$$

where k_{pp} and k_{pq} are the proportional coefficients, and k_{ip} and k_{iq} are the integral coefficients.

Fig. 3 shows the process of shifting droop curves. When the inverter operates at a rated point, the output voltage amplitude is U_0, the frequency is f_0, and the output active and reactive powers are P_0 and Q_0, respectively. For example, the inverter initially operates at point a, as shown in Fig. 3(a). The grid frequency is subsequently assumed to change from f_0 to f_1. The new operating point of the inverter will be at b because the frequency of the inverter is forced by the grid. However, to keep the output active power constant, the P–f droop curve should be shifted dynamically from curve 1 to curve 2. At this point, the new operating point of the inverter changes to c. Hence, the output frequency is f_1 and the output active power is P_0 at a steady state. A proportional–integral (PI) controller is used to maintain the shifting value of the inverter's frequency.

The same procedure applies to Fig. 3(b), where the initial reactive power Q_0 must be maintained while shifting the inverter voltage from U_0 to U_1. Therefore, the operating point is forced to change from a to c, where the output voltage amplitude is U_1 while active power is Q_0 at a steady state. Moreover, another PI controller is used to maintain the shifting value of the inverter's output voltage.

Expressions (9) and (10) are added to (11) and (12); thus, the droop expressions in grid-connected mode can be obtained as

$$f = f_0 + (k'_{pp} + \frac{k'_{ip}}{s})(P_0 - P), \tag{13}$$

$$U = U_0 + (k'_{pq} + \frac{k'_{iq}}{s})(Q_0 - Q), \tag{14}$$

where k'_{pp} and k'_{pq} are the proportional coefficients, and k'_{ip} and k'_{iq} are the integral coefficients.

If only positive-sequence components are considered under an imbalanced grid voltage, then the corresponding droop expressions can be derived as

$$f = f_0 + (K_{pp} + \frac{K_{ip}}{s})(P_0^+ - P^+), \tag{15}$$

$$U = U_0 + (K_{pq} + \frac{K_{iq}}{s})(Q_0^+ - Q^+), \tag{16}$$

where K_{pp} and K_{pq} are the proportional coefficients, and K_{ip} and K_{iq} are the integral coefficients.

IV. Improved Voltage-type Unbalance Compensation Control

A. Control Scheme

The positive-sequence fundamental active and reactive powers can be controlled under an imbalanced grid voltage by using (15) and (16). However, the negative-sequence reactive power Q^- is not effectively suppressed. The negative-sequence component not only damages the local load but also influences the stable operation of the grid-connected inverter. The unbalanced effects caused by the negative-sequence reactive component cannot be ignored, especially when inverter capacity is large.

To solve the aforementioned issues, an improved droop control is proposed based on the positive-sequence power droop control. VUF is reduced by adding a negative-sequence reactive power conductance (Q^-–G) loop. The negative-sequence reactive power is obtained by combining with the negative-sequence extraction as follows:

$$Q^- = u_\alpha^- i_\beta^- - u_\beta^- i_\alpha^-, \tag{17}$$

where u_α^- and u_β^- and i_α^- and i_β^- are negative sequence voltages and currents in a two-phase stationary coordinate system, respectively.

The negative sequence reactive conductance G^* is represented as

$$G^* = G_0 - mQ^-, \tag{18}$$

where G_0 is the rated conductance, which is set to zero in this study. m is the droop coefficient, which is determined by the negative-sequence reactive power of the inverter output.

The inverter can be controlled as an adjustable negative-sequence conductance in grid-connected mode by adding the Q^-–G loop. The equivalent conductance is proportionate to the negative-sequence reactive power produced by the inverter. Then, this conductance is multiplied by the negative-sequence PCC voltage to generate the compensation current reference. On the basis of the relation among voltage, current, and power, the compensating current can be obtained as

$$i_{o\alpha\beta}^- = G^* \cdot u_{o\alpha\beta}^-. \tag{19}$$

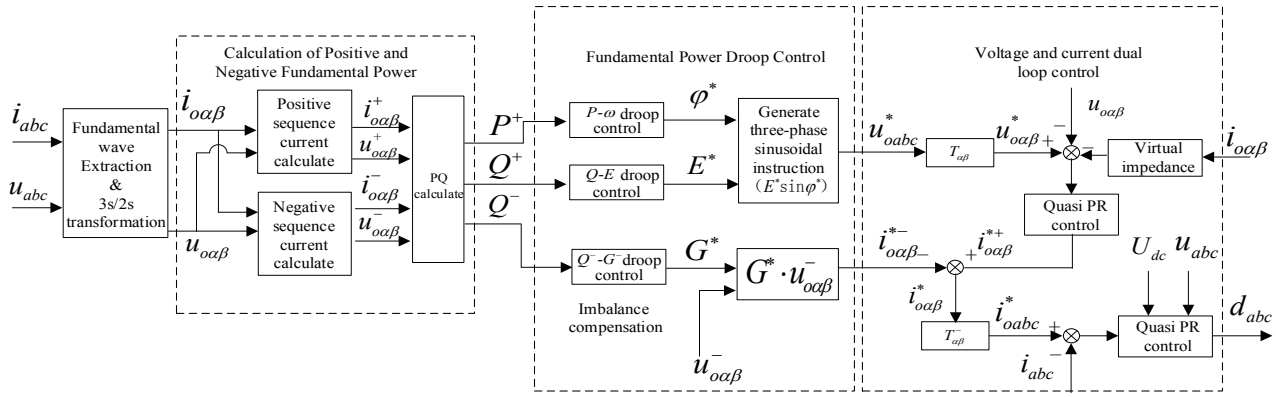

Fig. 4. Overview of improved droop scheme.

If the PCC voltage in grid-connected mode becomes unbalanced, then the negative-sequence reactive power will increase, thereby increasing equivalent conductance. Consequently, the compensation current will also increase. The grid current imbalance can be compensated, and the PCC voltage imbalance can be suppressed simultaneously.

Fig. 4 shows the eventual grid-connected scheme implemented for the three-phase inverter under an unbalanced grid. Typically, the voltages and currents in the stationary *a–b–c* frame is transformed into $i_{o\alpha\beta}$ *and* $u_{o\alpha\beta}$ in the stationary *α–β* frame using Clarke transformation $T_{\alpha\beta}$. Positive- and negative-sequence voltage and current can be obtained by using the positive- and negative-sequence extraction schemes, respectively. P^+, Q^+, and Q^- can then be calculated. The improved droop control loop generates the voltage reference and the negative-sequence current compensation reference. Finally, the voltage and current dual-loop controller is used to generate the driving signals of the switches.

B. Small Signal Analysis

Small signal analysis is performed next on the voltage and current dual-loop controller to investigate the system stability influence of the conductance loop parameter *m*.

In accordance with the foregoing analysis, the current reference can be obtained as

$$\mathbf{i}^* = -m \cdot \mathbf{u_0^-} \cdot Q^- , \tag{20}$$

where u_o^- is the inverter output negative-sequence voltage.

The output impedance at the fundamental frequency Z_o is approximately equal to $L_v s$ by adding the virtual impedance loop. Thus, the negative-sequence reactive power at the fundamental frequency can be derived as

$$Q^- = 3 \cdot X_v \cdot (I_o^-)^2 , \tag{21}$$

where X_v is the virtual reactance designed by the virtual impedance loop, and I_o^- is the fundamental negative-sequence component of the inverter output current. Equation (22) can be obtained by substituting (20) into (21).

$$\mathbf{i}^* = -3 \cdot m \cdot \mathbf{u_0^-} \cdot X_v \cdot (I_o^-)^2 \tag{22}$$

Thus, the linearly perturbed expression for the current reference is derived as

$$\hat{\mathbf{i}}^* = -[3 \cdot \mathbf{u_0^-} \cdot X_v \cdot (\mathbf{I_0^-})^2 + 6 \cdot \mathbf{u_0^-} \cdot X_v \cdot \mathbf{I_0^-} \cdot \hat{\mathbf{I}}_\mathbf{0}^-] \cdot m . \tag{23}$$

In general, the load impedance of a system is considerably larger than the line impedance; hence, the negative-sequence current can be approximately obtained as

$$\mathbf{I_0^-} \approx \frac{\mathbf{E}^*}{Z_L(j\omega)} , \tag{24}$$

where Z_L is the load impedance. Similarly, the negative-sequence voltage is given by

$$\mathbf{u_0^-} \approx -Z_o^-(j\omega) \cdot \mathbf{I_0^-} . \tag{25}$$

When (24) is substituted into (21), the following expression can be obtained:

$$\hat{\mathbf{i}}^* = -[\frac{3 \cdot X_v \cdot (\mathbf{E}^*)^2}{Z_L^2(j\omega)} \cdot \hat{\mathbf{u}}_\mathbf{0}^- + \frac{6 \cdot X_v \cdot (\mathbf{E}^*)^2 \cdot Z_o^-(j\omega)}{Z_L^2(j\omega)} \cdot \hat{\mathbf{I}}_\mathbf{0}^-] \cdot m . \tag{26}$$

The corresponding small signal perturbation model can be expressed as

$$\hat{\mathbf{u}}_\mathbf{0}^- = G_{closed\text{-}loop} \cdot \hat{\mathbf{I}}_\mathbf{0}^- , \tag{27}$$

where

$$G_{closed-loop} = \frac{6 \cdot G^-(j\omega) \cdot X_v \cdot Z_o^-(j\omega) \cdot m}{Z_L^2(j\omega) + 3G^-(j\omega) \cdot X_v \cdot m} - \frac{Z_o^-(j\omega) \cdot Z_L^2(j\omega)}{Z_L^2(j\omega) + 3G^-(j\omega) \cdot X_v \cdot m} . \tag{28}$$

The analysis of the small signal perturbation model of the negative sequence conductance loop suggests that a large droop coefficient *m* indicates that voltage unbalance compensation is evident. However, a large *m* value may lead to the instability of the system. Here, *m* = 0.0001, 0.002, 0.02, and 0.05 are selected to investigate the root locus. Fig. 5 shows the zero and pole distribution with different droop coefficients *m*. When *m* = 0.05, an unstable pole in the root locus is observed on the right half plane. When *m* = 0.001, 0.002, and 0.02, the zeros and poles are all on the left half

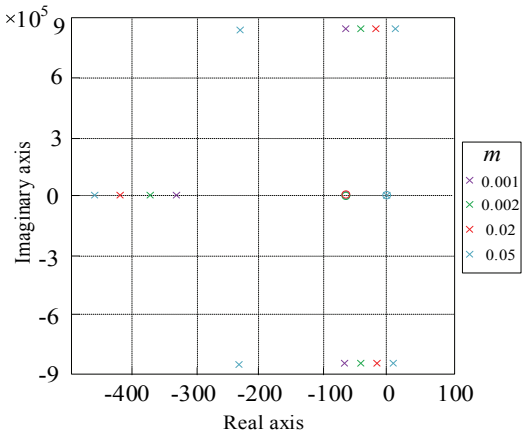

Fig. 5. Zero and pole distribution graphs with different droop coefficients *m*.

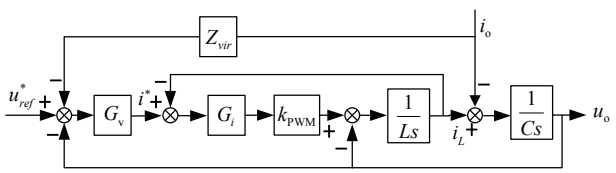

Fig. 6. Block diagram of control system and power stage.

plane, thereby showing that the system is stable. Consequently, *m* is set as 0.02 in this study.

C. Controller Design

Subsequently, the voltage–current dual loop, virtual impedance control loops, and droop controllers will be designed. The block diagram of the control system and power stage is shown in Fig. 6. The following equation can be obtained as

$$u_o = G(s)\cdot u_{ref} - Z(s)\cdot i_o \,, \tag{29}$$

$$G(s)=\frac{G_i(s)G_v(s)Ls}{L^2Cs^3+G_i(s)LCs^2+Ls-LG_i(s)G_v(s)s+2G_i(s)} \,, \tag{30}$$

$$Z(s)=\frac{G_i(s)G_v(s)Z_vLs+L^2s^2+LsG_i(s)}{L^2Cs^3+G_i(s)LCs^2+Ls-LG_i(s)G_v(s)s+2G_i(s)} \,, \tag{31}$$

where $G(s)$ and $Z(s)$ are the control system closed-loop transfer function and output impedance, respectively.

The Bode diagrams of $G(s)$ and $Z(s)$ are depicted in Figs. 7 and 8, respectively, by considering the power stage and primary control system parameters (listed in Tables I). In Fig. 7, the amplitude and phase angle of $G(s)$ at the fundamental frequency are zero, which indicates that the designed control system can perfectly track system input at the fundamental frequency. Fig. 8 shows the amplitude–frequency characteristic curve of $Z_o(s)$. The equivalent impedance $Z_o(s)$ is inductive at the fundamental frequency. Therefore, the decoupling between P^+ and Q^+ can be realized by using virtual impedance.

When connected to the utility grid, the droop controller

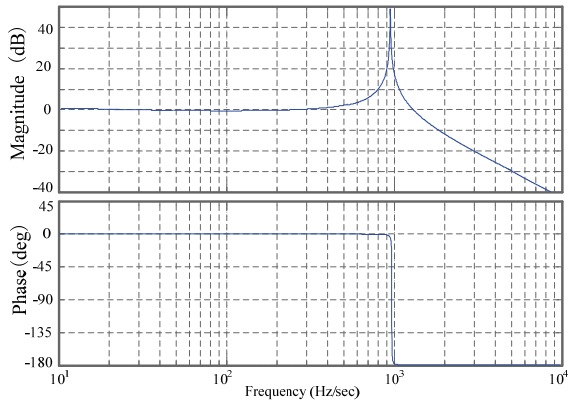

Fig. 7. Bode diagram of the closed loop transfer function.

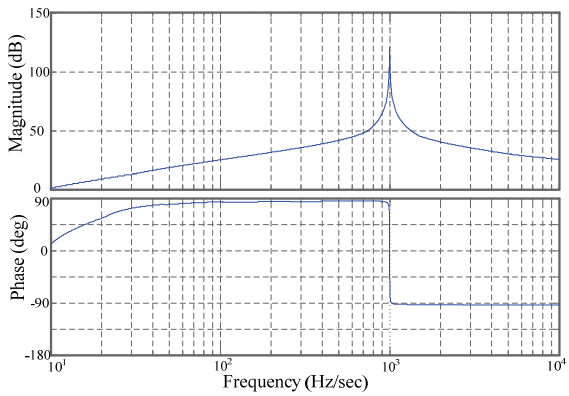

Fig. 8. Bode diagram of the equivalent output impedance.

based on the PI controller is used to force the active and reactive power output of the inverter to track its desired value with zero steady-state error. The parameters (k_{pp} = 0.0001, k_{ip} = 0.00001, k_{pq} = 0.002, k_{iq} = 0.001) are set to provide a sufficiently long response time, which is required to decouple the slow outer droop power loop from the fast inner voltage and current-tracking loops. When slight fluctuations occur in grid voltage amplitude and frequency, the control can change the droop characteristics for a constant active and reactive power injection into the grid, thereby ensuring a stable operation in grid-connected mode.

The compensation coefficient *m* of the negative-sequence conductance loop is designed based on the stability analysis shown in the previous section. Here, *m* is set as 0.02, such that the entire system is stable and receives a rapid, dynamic response.

V. Simulation and Experimental Results

A. Simulation Results

A three-phase grid-connected inverter system tied to an unbalanced grid is simulated in MATLAB/Simulink. The grid voltage is 220 V (RMS value), and the A-phase voltage is reduced from 220 V to 205 V. The conventional positive-sequence power droop is adopted before compensation, and

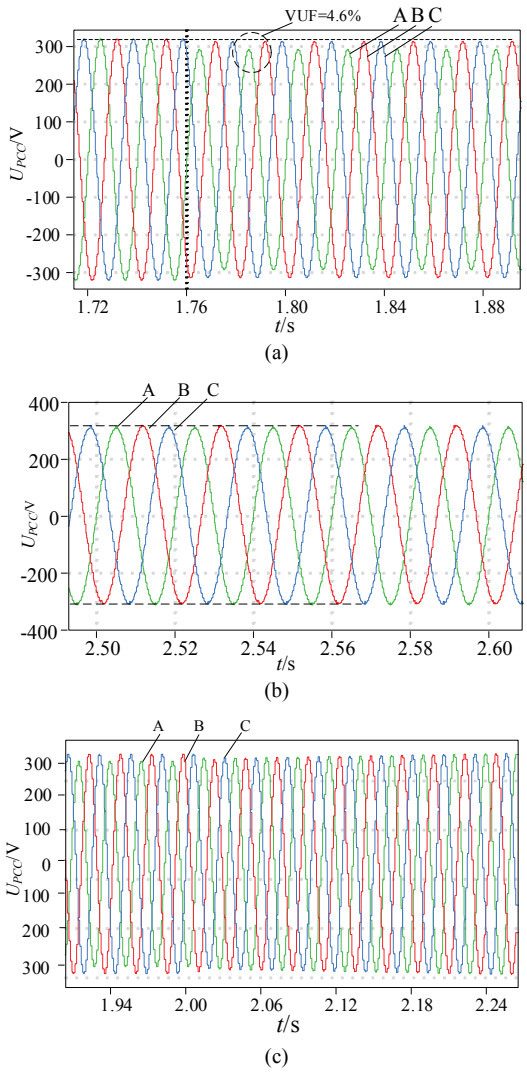

Fig. 9. Grid-connected voltage waveforms: (a) Before compensation, (b) After compensation, (c) During compensation.

droop control is proposed by adding the Q^{-}–G loop, which is adopted after compensation. Fig. 9(a) shows the PCC voltage before the use of power compensation. The three-phase voltage imbalance phenomenon occurs at 2 s, and VUF is equal to 4.6%. Fig. 9(b) shows the simulation results when the proposed control scheme is used. VUF is reduced to 1%, and PCC voltage is basically maintained at 220 V from 2 s to 4 s. Hence, the proposed scheme can efficiently compensate for the unbalance voltage at PCC. The dynamic process during compensation is shown in Fig. 9(c). PCC voltage can be compensated rapidly to balance the state, and phase A voltage is significantly supported by 15 V.

The current waveforms before, after, and during compensation is shown in Fig. 10. The B-phase current, which realizes unbalanced current compensation, exhibits a significant increase after compensation. Fig. 11 shows the simulation results of the positive- and negative-sequence powers under grid fault condition. After adding droop power

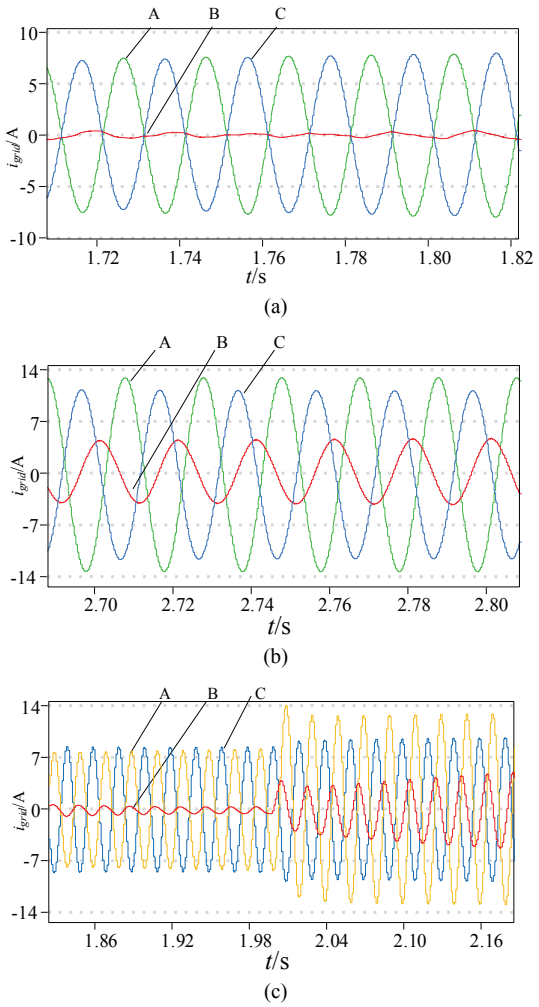

Fig. 10. Grid connected current waveforms: (a) Before compensation, (b) After compensation, (c) During compensation.

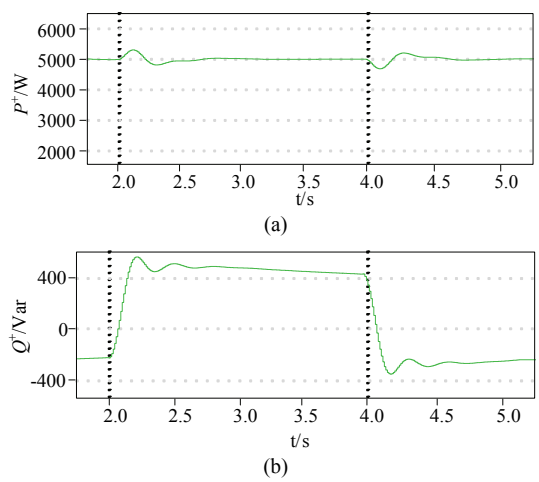

Fig. 11. Simulation results: (a) Positive-, (b) Negative-sequence powers.

control, the positive-sequence active power is maintained at 5000 W. Simultaneously, th inverter output reactive power increases to 500 Var due to the need to compensate the PCC

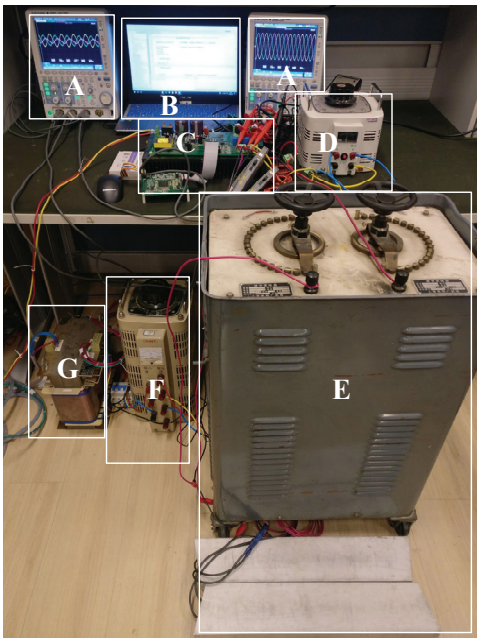

Fig. 12. Laboratory setup: A - oscilloscope, B - laptop, C - three-phase inverter, D – single-phase voltage regulator, E - load, F - 220 V/110 V three-phase voltage regulator, and G - isolation transformer tied to a grid.

TABLE I
PARAMETERS OF THE THREE-PHASE GRID-CONNECTED INVERTER

Parameters	Values
Active droop coefficients (K_{pp})	0.0001
Active droop coefficients (K_{ip})	0.00001
Reactive droop coefficients (K_{pq})	0.002
Reactive droop coefficients (K_{iq})	0.001
Voltage loop PR parameters (k_{pu}, k_{ru})	0.08,20
Current loop PR parameters (k_{pi}, k_{ri})	3,200
Virtual impedance	4 mH
Compensation coefficient (m)	0.02
Voltage unbalance factor (VUF)	5.3%
Output filter inductance (L)	8 mH
Output filter capacitance (C)	4.7 uF
Impedance of transmission line (L_g)	4 mH
Local load (Z_L)	48.4 Ω
DC-link voltage(U_{dc})	400V

voltage caused by the unbalanced grid. The response time of compensation is within 0.4 s, which demonstrates the excellent dynamic performance of the proposed scheme.

B. Experimental Results

Experimental testing using a 1500 W grid-connected system (Fig. 12) is performed to prove the practicality of the proposed scheme, and its parameters are listed in Table I. In the experimental setup, a voltage regulator is cascaded between phases B and C after the grid. An unbalanced grid fault condition can be simulated by adjusting the turn ratio of the voltage regulator. Grid voltage is 110 V (RMS value), power frequency is 50 Hz, and switching frequency is 10 kHz.

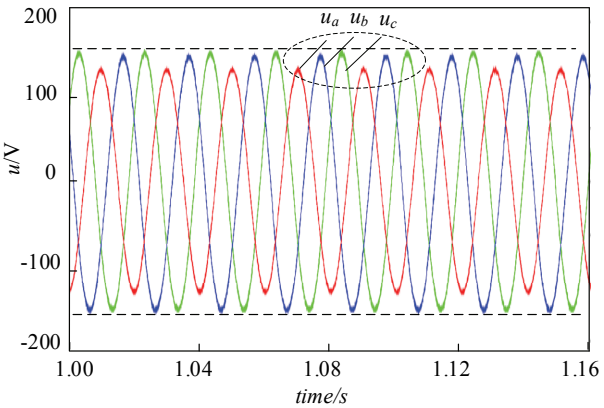

Fig. 13. Waveform of an unbalanced grid voltage.

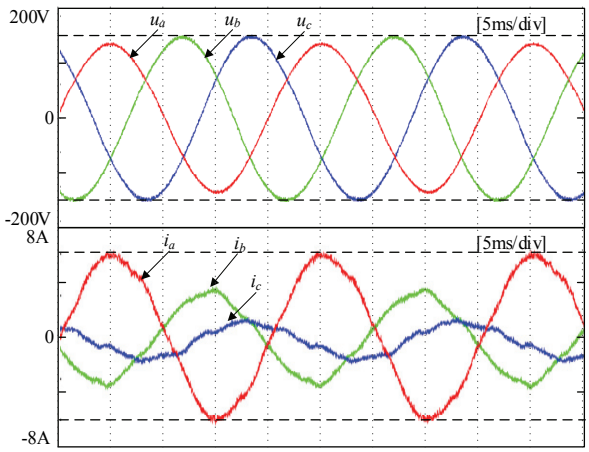

Fig. 14. Experimental results of grid-connected voltage when the positive-sequence power droop control is used.

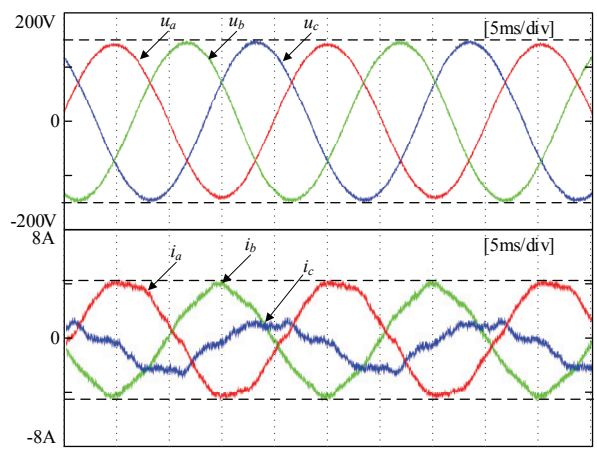

Fig. 15. Experimental results of grid-connected current when the improved droop control scheme is used.

Fig. 13 shows the experimental fault condition setup of the three-phase grid voltages. The B and C phase voltages are 155 V (peak value), which is 23 V higher than A phase voltage. The unbalance factor is approximately 5.3%.

Fig. 14 shows the experimental results when the positive-sequence power droop control is used, i.e., the results before compensation. U_a is 140 V, which is lower than U_b and U_c (155 V). The unbalance factor is maintained at approximately 4.2%. The amplitude of phases B and C current are 4.0 A and 1.2 A, respectively. Furthermore, the amplitude of phase A current I_a is larger than 5 A, which exceeds the upper limit of the output current for compensating an unbalanced grid voltage. Evidently, the three phase injected currents are seriously unbalanced.

Fig. 15 shows the three-phase PCC voltage and current waveforms when the improved droop control scheme is used, i.e., the results after compensation. VUF is reduced to 1.5%, and the amplitude difference of the three-phase PCC voltage is decreased compared with that in Fig. 14. Moreover, the system can operate stably. The C phase current, which is seriously unbalanced before compensation, is considerably increased to 1.8 A due to the decrease in the negative- sequence reactive power. Simultaneously, the currents of phases A and B decrease to 4.1 A, thereby avoiding overcurrent. The unbalance factor of the three-phase grid current is significantly reduced after compensation. The experimental results verify that the proposed control strategy can compensate for voltage drop and reduce the grid current unbalance factor under an unbalanced grid voltage condition, thereby ensuring the safe and reliable operation of grid- connected inverters.

VI. CONCLUSIONS

An improved droop control is proposed in this study to suppress voltage imbalance at PCC. The proposed control scheme includes an unbalance compensating loop, active and reactive power droop control loops, and voltage and current control loops. The compensating loop regulates the positive- and negative-sequence output reactive powers of the inverter, which ensures that PCC voltage is controlled within allowable limits. The design and stability analysis of the control system are discussed. The proposed control strategy can maintain the stable operation of the inverter under an unbalanced grid condition. The simulation and experimental results verify the performance of the proposed method.

REFERENCES

[1] A. Camacho, M. Castilla, J. Miret, P. Marti, and M. Velasco, "Maximizing positive sequence voltage support in inductive-resistive grids for distributed generation inverters during voltage sags," in *Proc. IECON*, pp. 2343-2348, 2016.

[2] Y. Suh and T. A. Lipo, "Control scheme in hybrid synchronous stationary frame for PWM AC/DC converter under generalized unbalanced operating conditions," *IEEE Trans*. *Ind. Appl*., Vol. 42, No. 3, pp. 825-835, May/Jun. 2006.

[3] M. Reyes, P. Rodriguez, S. Vazquez, A. Luna, R. Teodorescu, and J. M. Carrasco, "Enhanced decoupled double synchronous reference frame current controller for unbalanced grid-voltage conditions," *IEEE Trans*. *Power Electron*., Vol. 27, No. 9, pp. 3934-3943, Sep. 2012.

[4] X. Wang, X. Ruan, S. Liu, and C. K. Tse, "Full feed-forward of grid voltage for grid-connected inverter with LCL filter to suppress current distortion due to grid voltage harmonics," *IEEE Trans*. *Power Electron*., Vol. 25, No. 12, pp. 3119-3127, Dec. 2010.

[5] R. Rodriguez, A. V. Timbus, R. Teodorescu, M. Liserre, and F. Blaabjerg, "Flexible active power control of distributed power generation systems during grid faults," *IEEE Trans*. *Ind. Electron*., Vol. 54, No. 5, pp. 2583-2592, Oct. 2007.

[6] A. Camacho, M. Castilla, J. Miret, R. Guzman, and A. Borrell, "Reactive power control for distributed generation power plants to comply with voltage limits during grid faults," *IEEE Trans*. *Power Electron*., Vol. 29, No. 11, pp. 6224-6234, Nov. 2014.

[7] A. A. Montanari and A. M. Gole, "Enhanced instantaneous power theory for control of grid connected voltage sourced converters under unbalanced conditions," *IEEE Trans*. *Power Electron*., Vol. 32, No. 8, pp. 6652-6660, Aug. 2017.

[8] J. M. Guerrero, J. C. Vasquez, J. Matas, L. G. de Vicuna, and M. Castilla, "Hierarchical control of droop-controlled AC and DC microgrids – A general approach toward standardization," *IEEE Trans*. *Ind. Electron*., Vol. 58, No. 1, pp. 158-172, Jan. 2011.

[9] H. Bevrani and S. Shokoohi, "An intelligent droop control for simultaneous voltage and frequency regulation in islanded microgrids," *IEEE Smart Grid*, Vol. 4, No. 3, pp. 1505-1513, Sep. 2013.

[10] Q. C. Zhong and G. C. Konstantopoulos, "Current-limiting droop control of grid-connected invertes," *IEEE Trans*. *Ind. Electron*., Vol. 64, No. 7, pp. 5963-5973, Jul. 2017.

[11] R. R. Kolluri, I. Mareels, T. Alpcan, J. de Hoog, and D. A. Thomas, "Power sharing in angle droop controlled microgrids," *IEEE Trans*. *Power Syst*., Vol. 32, No. 6, pp. 4743-4751, Nov. 2017.

[12] M. Hamzeh, H. Karimi, and H. Mokhtari, "A new control strategy for a multi-bus MV microgrid under unbalanced conditions," *IEEE Trans*. *Power Syst*., Vol. 27, No. 4, pp. 2225-2232, Nov. 2012.

[13] X. Zhao, J. M. Guerrero, M. Savaghebi, J. C. Vasquez, X. H. Wu, and K. Sun, "Low-voltage ride-through operation of power converters in grid-interactive microgrids by using negative-sequence droop control," *IEEE Trans*. *Power Electron*., Vol. 32, No. 4, pp. 3128-3142, Apr. 2017.

[14] N. R. Merritt, C. Chakraborty, and P. Bajpai, "New voltage control strategies for VSC-based DG units in an unbalanced microgrid," *IEEE Trans*. *Sustain. Energy*, Vol. 8, No. 3, pp. 1127-1139, Jul. 2017.

[15] M. Mirhosseini, J. Pou, and V. G. Agelidis, "Individual phase current control with the capability to avoid overvoltage in grid-connected photovoltaic power plants under unbalanced voltage sags," *IEEE Trans*. *Power Electron*., Vol. 30, No. 10, pp. 5346-5351, Oct. 2015.

[16] X. Q. Guo, W. Z. Liu, X. Zhang, X. F. Sun, Z. G. Lu, and J. M. Guerrero, "Flexible control strategy for grid-connected inverter under unbalanced grid faults without PLL," *IEEE Trans*. *Power Electron*., Vol. 30, No. 4, pp. 1773-1778, Apr. 2015.

[17] A. Camacho, M. Castilla, J. Miret, J. C. Vasquez, and E. Alarcon-Gallo, "Flexible voltage support control for three-phase distributed generation inverters under grid fault," *IEEE Trans. Ind. Electron.*, Vol. 60, No. 4, pp. 1429-1441, Apr. 2013.
[18] X. Q. Guo, X. Zhang, B. C. Wang, W. Y. Wu and J. M. Guerrero, "Asymmetrical grid fault ride-through strategy of three-phase grid-connected inverter considering network impedance impact in low-voltage grid." *IEEE Trans. Power Electron.*, Vol. 29, No. 3, pp. 1064-1068, Mar. 2014.
[19] M. Ciobotaru, R. Teodorescu, and F. Blaabjerg, "A new single-phase PLL structure based on second order generalized integrator," in *Proc. IEEE PESC*, pp. 1-6, 2006.

Hongpeng Liu was born in Inner Mongolia, China. He obtained his B.S. in Electrical Engineering from Harbin University of Science and Technology, Harbin, China, in 2000, and his M.S. and Ph.D. in Electrical Engineering from Harbin Institute of Technology, Harbin, China, in 2006 and 2011, respectively. In 2011, he joined Harbin Institute of Technology as an assistant professor in the Department of Electrical Engineering, where he has served as an associate professor since December 2016. His current research interests include photovoltaic generation, microgrids, and pulse-width modulation converter/inverter systems.

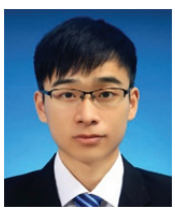

Jiajie Zhou was born in Zhejiang Province, China. He obtained his B.S. in Electrical Engineering from Harbin Institute of Technology, Harbin, China in 2016. He is currently working toward an M.S. in Electrical Engineering at Harbin Institute of Technology, Harbin, China. His current research interests include photovoltaic generation and control of three/single-phase inverters.

Wei Wang was born in Heilongjiang Province, China. She obtained her B.S. in Automatic Test and Control from Harbin Institute of Technology, Harbin, China in 1984, her M.S. in Electrical Engineering from Harbin Institute of Technology in 1990, and her Ph.D. in Mechanical Electronic Engineering from Harbin Institute of Technology in 2002. In 1984, she joined Harbin Institute of Technology as an assistant professor in the Department of Electrical Engineering, where she has served as an associate professor from 1995 to 2003 and as a professor since 2003. Her current research interests include regenerative energy converter techniques, microgrids, soft-switching converters, and electronic lighting technology.

Dianguo Xu was born in Heilongjiang Province, China. He obtained his B.S. in Control Engineering from Harbin Shipbuilding Engineering Institute, Harbin, China, in 1981, and his M.S. and Ph.D. in Electrical Engineering from Harbin Institute of Technology (HIT), Harbin, China, in 1984 and 1990, respectively. In 1984, he joined HIT as an assistant professor in the Department of Electrical Engineering, where he has served as an associate professor from July 1991 to June 1994 and as a professor since July 1994. He was the dean of the School of Electrical Engineering and Automation, HIT from 2000 to 2010 and was the assistant president of HIT from 2010 to 2014. He is currently the vice president of HIT. His current research interests include renewable energy generation technology, power quality mitigation, sensorless vector controlled motor drives, and high-performance permanent magnet synchronous motor servo systems.